Interlayer Magnetic Interaction in the $CrI_3/CrSe_2$ Heterostructure

Qiu-Hao Wang(王秋皓)[1,2,3], Mei-Yan Ni(倪美燕)[1], Shu-Jing Li(李淑静)[4], Fa-Wei Zheng(郑法伟)[2,3], Hong-Yan Lu(路洪艳)[1*], and Ping Zhang(张平)[1,5*]

[1]*School of Physics and Physical Engineering, Qufu Normal University, Qufu 273165, China*
[2]*Center for Quantum Physics, Key Laboratory of Advanced Optoelectronic Quantum Architecture and Measurement (MOE), School of Physics, Beijing Institute of Technology, Beijing 100081, China*
[3]*Beijing Key Lab of Nanophotonics and Ultrafine Optoelectronic Systems, School of Physics, Beijing Institute of Technology, Beijing 100081, China*
[4]*College of Mathematics and Physics, Beijing University of Chemical Technology, Beijing 100029, China*
[5]*Institute of Applied Physics and Computational Mathematics, Beijing 100088, China*

(Received 29 January 2024; accepted manuscript online 2 April 2024)

Based on first-principles calculations, we systematically study the stacking energy and interlayer magnetic interaction of the heterobilayer composed of CrI_3 and $CrSe_2$ monolayers. It is found that the stacking order plays a crucial role in the interlayer magnetic coupling. Among all possible stacking structures, the AA-stacking is the most stable heterostructure, exhibiting interlayer antiferromagnetic interactions. Interestingly, the interlayer magnetic interaction can be effectively tuned by biaxial strain. A 4.3% compressive strain would result in a ferromagnetic interlayer interaction in all stacking orders. These results reveal the magnetic properties of $CrI_3/CrSe_2$ heterostructure, which is expected to be applied to spintronic devices.

DOI: 10.1088/0256-307X/41/5/057401

Since the successful fabrication of graphene [1] in 2004, research on two-dimensional (2D) materials has been growing rapidly. Lately, the discoveries of atomically thin CrI_3 [2] and $Cr_2Ge_2Te_6$ [3] draw much attention to investigations of 2D magnets. The CrI_3 monolayer has a very simple atomic structure and relatively strong magnetic anisotropy, which removes the striction of Mermin–Wagner's theorem resulting in a 45 K Curie temperature T_c. Recently, another 2D magnet, [4] $CrSe_2$ monolayer, with another very simple atomic structure and a higher T_c (110 K) was found. The morphology and magnetic properties of $CrSe_2$ monolayer stay unchanged even after several months of exposure to air. The notable stability inspires more studies on its spintronic device applications.

In designs of spintronic devices, the interlayer magnetic interaction plays a crucial role in bilayer or multilayer magnetic materials. The interlayer magnetic interaction in bilayer CrI_3 has been extensively studied. [5–12] The bilayer CrI_3 obtained by stripping from the bulk CrI_3 still maintains ferromagnetism (FM) in the layer, while the interlayer coupling is antiferromagnetic (AFM). The interlayer AFM coupling can be transformed into FM coupling by interlayer slip, [13] twisted bilayer, [14] and applied magnetic field. [15,16] The interlayer magnetic interaction in bilayer $CrSe_2$ is also studied lately. In bilayer $CrSe_2$, interlayer slip and twisted structures [17] also achieve interlayer coupling transition. However, the interlayer magnetic interaction in heterobilayer magnetic materials has rarely been studied. To our knowledge, only a few heterobilayer magnets have been studied. [18] Actually, the heterobilayer structure largely enriches the family of bilayers, shows rich phenomena, and provides more versatility in designs of spintronic devices.

In this Letter, we construct a heterostructure of CrI_3 and $CrSe_2$ monolayers, and study the effect of stacking order and strain on the interlayer magnetic interaction. We demonstrate that the interlayer magnetic interaction varies significantly, and can be either FM or AFM, depending on the stacking order when the lattice constant is 7.3 Å. Oppositely, the interlayer magnetic interaction is very robust FM when the lattice constant is 7.0 Å. This sensitivity to the lattice constant comes from the abrupt decrease of the nearest neighboring AFM interaction when the lattice constant is in the range of 7.15–7.25 Å.

The atomic structures and the magnetic interactions of the $CrI_3/CrSe_2$ heterostructure are studied by using the density functional theory (DFT) [19,20] calculation method. The exchange-correlation functional is approximated by using the Perdew–Burke–Ernzerhof [21] form of the generalized gradient approximation, and the core electrons are described by the projector augmented wave [22,23] method. The plane wave cutoff energy is 300 eV. The reciprocal space is integrated on an $8 \times 8 \times 1$ Monkhorst–Pack K-mesh. A 2.8 eV of Hubbard-U correction is adopted in the DFT+U [24] calculations to correctly describe the Cr d electrons. In order to accurately calculate the interlayer coupling, we also use the D3 vdW correction method. [25] Atomic structures are relaxed until the residual forces are smaller than 1×10^{-3} meV/Å. A 15 Å vacuum space is employed to avoid the spurious interaction between periodic images. All the DFT calculations are performed using the Vienna *ab initio* simulation package (VASP). [26]

The lattice constant of monolayer CrI_3 is 7.00 Å, [2] which is approximately twice the lattice constant of the

*Corresponding authors. Email: hylu@qfnu.edu.cn; zhang_ping@iapcm.ac.cn
© 2024 Chinese Physical Society and IOP Publishing Ltd

monolayer $CrSe_2$ (3.63 Å [4]). Therefore, we construct the computational cell of the heterobilayer with a primitive cell CrI_3 monolayer and a 2×2 supercell $CrSe_2$ monolayer. The lattice mismatch is only about 3.3%. Therefore, we use two lattice constants to simulate a slightly stretched and compressed heterobilayer, which are 7.3 Å and 7.0 Å, respectively. The interlayer distance in both the cases are within a reasonable range, which are 3 Å and 3.3 Å, respectively.

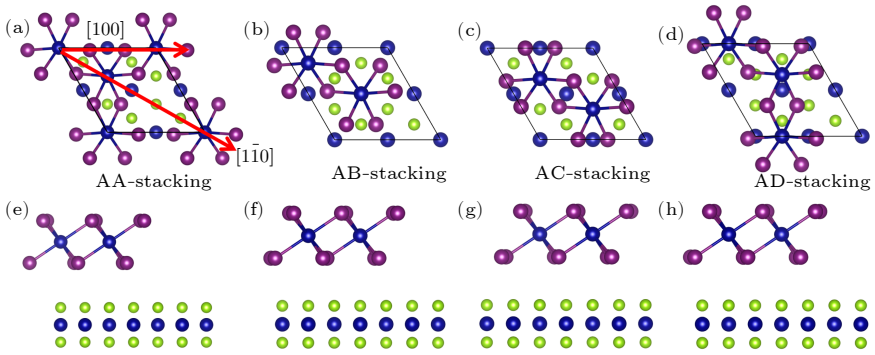

Fig. 1. The top (a)–(d) and side (e)–(h) views of AA-stacking, AB-stacking, AC-stacking, and AD-stacking configurations of the $CrI_3/CrSe_2$ heterostructure. The blue, green, and purple atoms represent the Cr, Se, and I atoms, respectively.

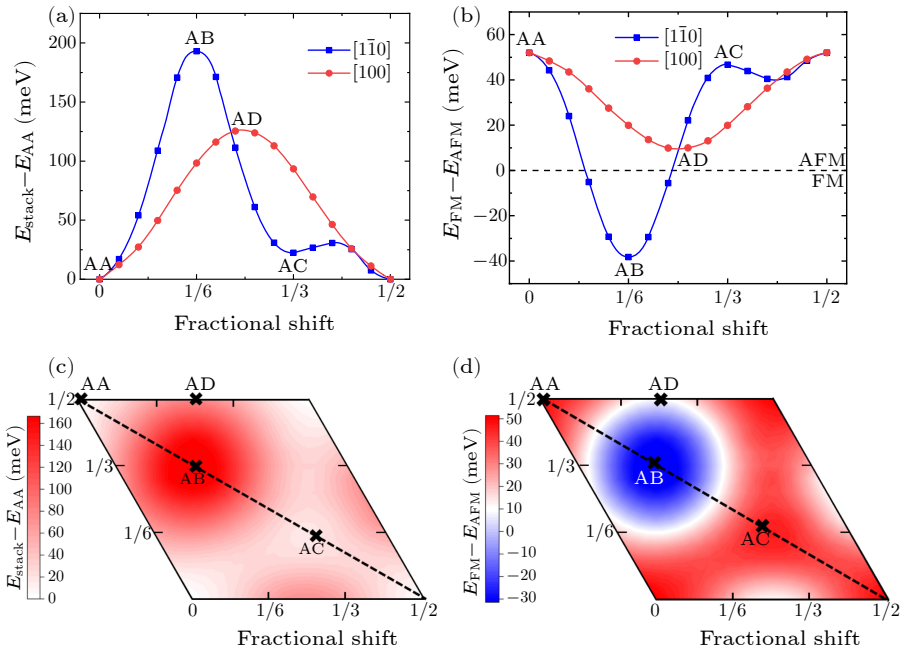

Fig. 2. Effect of interlayer shift on (a) stacking energy and (b) interlayer exchange energy when the lattice constant is 7.3 Å of the $CrI_3/CrSe_2$ heterostructure. The blue line is in the [1$\bar{1}$0] direction, the red line is in the [100] direction. The stacking energy (c) and interlayer exchange energy (d) for the full space of lateral shift. In (d), red and blue regions represent AFM and FM couplings, respectively.

We shift the CrI_3 monolayer respect to the $CrSe_2$ monolayer to get all possible stacking orders. Since its underlying structure is the 2×2 supercell of $CrSe_2$, a repeating process will be generated when it slides along the direction of a high symmetry line, thus we only need to study half of the distance to understand the whole process. We consider the transverse shift of the top layer CrI_3 along the direction of two highly symmetrical lines [1$\bar{1}$0] and [100]. We define the initial structure as AA-stacking, 1/6 shift along [1$\bar{1}$0] direction as AB-stacking, and 1/3 shift along [1$\bar{1}$0] direction as AC-stacking. The top and side views of AA-stacking, AB-stacking, and AC-stacking are shown in Fig. 1. Along the direction [100], we define 1/4 shift of the top layer CrI_3 as AD-stacking. We define the stacking energy as the difference between the energy of the special stacking and the energy of the AA-stacking structure. In Fig. 2, we show the stacking energy of the case in lattice constant 7.3 Å. It is clear that shifting along [1$\bar{1}$0] direction, AA-stacking shows the lowest stacking energy, and AB-stacking shows the highest stacking energy. Shifting from AB-stacking to AC-stacking, the stack energy decreases gradually. When the stack energy exceeds AC-stacking, a local maximum value appears. Along the [100] direction, AA-stacking and AD-stacking show that

the lowest and highest stacking energies, respectively. Figure 2(c) shows the effect of interlayer shift on stacking energy in the whole plane, in which the corresponding special points are marked.

In addition, we also study the effect of high symmetric line shifts on the exchange energy of the heterostructure, which is defined as the energy difference between the FM and AFM states, with positive indicating AFM coupling and negative indicating FM coupling. The red curve in Fig. 2(b) represents the shift results along the [100] direction. The entire red curve is located in the AFM coupling region. The minimum exchange energy is 9.9 meV in the AD-stacking, and the maximum exchange energy is 52.0 meV in the AA-stacking. This shows that the interlayer coupling of the material does not change during the shift in the direction of [100]. The blue line represents a significant change in interlayer coupling along the $[1\bar{1}0]$ direction. The AA-stacking still show the highest exchange energy, but the interlayer coupling changes from AFM coupling to FM coupling, and the exchange energy will reach the lowest value of −38.2 meV at the AB-stacking. By further shifting to AC-stacking, the interlayer coupling changes from FM coupling to AFM coupling. The exchange energy of AC-stacking is 40.4 meV. The results show that the interlayer coupling changes from AFM coupling to FM coupling and back to AFM coupling during the $[1\bar{1}0]$ direction shift. Similarly, the effect of interlayer shift on the exchange energy in the whole plane is studied, and the results are shown in Fig. 2(d). The red area represents the layer interaction of AFM coupling, and the blue area is FM coupling. The results show that the FM coupling region exists around 1/6 of the shift in the $[1\bar{1}0]$ direction, and the other regions are AFM coupling.

Previous studies [27] have shown that the superposition of interlayer atomic positions leads to valley polarization. Similarly, the superposition of atomic positions may also affect changes in interlayer coupling. After our calculation, the closer the Se atoms near the interlayer region are to the top Cr atoms, the more favorable it is for antiferromagnetic coupling, while the greater the distance, the more conducive it is to the production of ferromagnetic coupling.

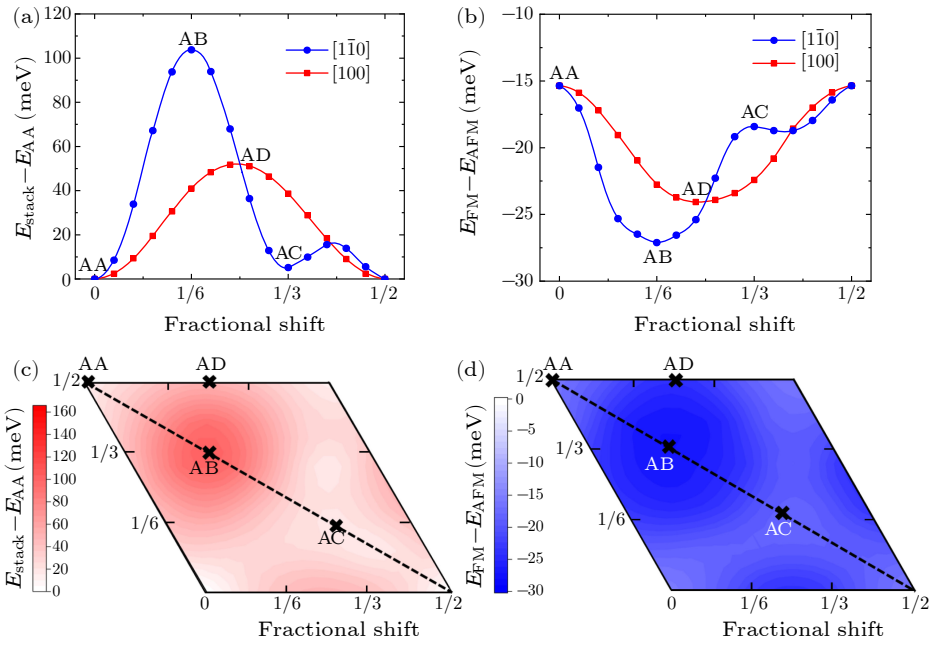

Fig. 3. Similar to Fig. 2 but for different lattice constant (7 Å) of $CrI_3/CrSe_2$ heterostructures.

The lattice constant (7.3 Å) we used in Fig. 2 is closer to $CrSe_2$ supercells, thus we continue to use 7 Å (the lattice constant of CrI_3 unit cell) to study the changes of stacking energy and exchange energy in different stacking orders. The results are shown in Figs. 3(a) and 3(c). The trend of change is consistent with the results in Figs. 2(a) and 2(c), but there are differences in values. The system with the highest stacking energy is still the AB-stacking order, the difference from AA-stacking is 103.7 meV, while the AA-stacking order has the lowest stacking energy, and it is the most stable state in the whole shifting process. The change of exchange energy for the case of 7 Å is also studied, and the results are shown in Fig. 3(b). The variation trend is similar to that in Fig. 2(b). It is worth noting that when the lattice constant is 7 Å, and the red and blue lines in the figure are both negative, indicating that the interlayer coupling of the material is FM coupling under this condition. The same result is shown in Fig. 3(d), where the entire region is blue, indicating that the interlayer coupling of the sliding material in any direction is FM coupling. Although the high stacking energy is not conducive to the existence of materials, the layers are constrained by the vdW force, and the strength is weak, we can still change the stacking order of materials by applying external forces.

By studying the effect of biaxial strain on the stacking energy and exchange energy of $CrI_3/CrSe_2$ heterostructure, we find that the variation of the lattice constant does

not change the trend of the correlation curves. Therefore, we believe that the shift along the high symmetry directions will still maintain the original trend under biaxial strain. However, the qualitative results of exchange energy under two different lattice constants are very different, thus we further study the exchange energy of different lattice constants. Two special stacking orders are selected as an example of the maximum value of exchange energy (AA-stacking) and the minimum value (AD-stacking), and the results are shown in Fig. 4(a). The blue line represents changes in the exchange energy of AA-stacking under different lattice constants, and the red line represents AD-stacking. When the lattice constant is 7 Å, the magnetic ground state of the heterostructure does not change no matter how they shift along the two highly symmetric lines, and the interlayer coupling shows an FM state. However, when the lattice constant increases to about 7.17 Å, the magnetic ground state transition will occur along the high symmetry line $[1\bar{1}0]$ and [100], and when the lattice constant continues to increase to 7.27 Å, the shift will completely change into an AFM state along the direction [100].

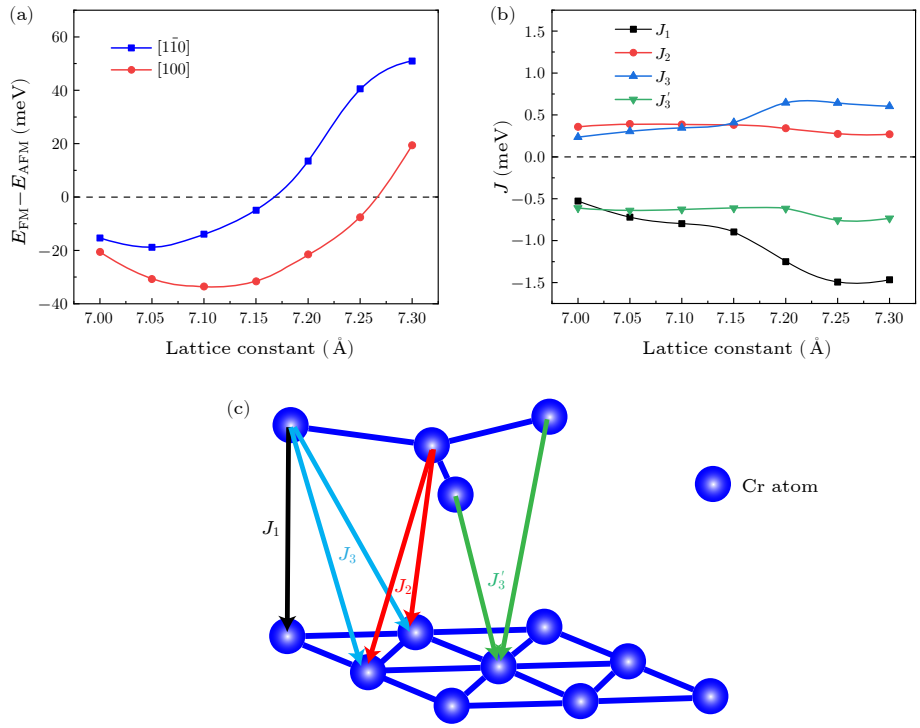

Fig. 4. (a) Stacking energy of AA-stacking and AD-stacking under different lattice constants, represented by blue and red lines, respectively. (b) The exchange parameter between magnetic atoms of different layers varies with the lattice constant. (c) Interaction between magnetic atoms of different layers.

This shows that this heterostructure is very sensitive to the change in strains. If we need a material that can be slid along two highly symmetric lines and shows magnetic ground state transition, we can control the lattice constant the of $CrI_3/CrSe_2$ heterostructure between 7.17 Å and 7.27 Å to achieve the desired properties. Shared strain [28] may occur in bilayer structures with slightly different lattice constants, as well as in molar patterns. In the real $CrI_3/CrSe_2$ system, the deviation of the ratio from contact 2 would lead to a moire pattern in a large scale. As previously reported in other moire systems, the local structures of this moire pattern can be described by the stacking structures studied in this work. Since the interlayer exchange interactions can be tuned by stacking, we can reach the conclusion that the moire potential would lead to a periodic tuning of the interlayer exchange interactions. This periodic interlayer exchange interactions would result in a moire pattern of the magnetic structure.

To find out the reason for the AFM interaction in the AA-stacking order, we continue to construct the Hamiltonian of the system. Here, we take the Heisenberg model, the Heisenberg Hamiltonian of the $CrI_3/CrSe_2$ heterostructure can be written as

$$H = H_i + H_0, \tag{1}$$

$$H_i = -\sum_{i,j} J_{i,j} S_i^{\rm u} \cdot S_j^{\rm d}. \tag{2}$$

The Hamiltonian is made up of the Hamiltonian H_0 within the layers and the H_i between the layers. $J_{i,j}$ represents the coupling parameters between the i-th Cr atom and the j-th Cr atom, and $S_i^{\rm u}$ and $S_j^{\rm d}$ represent the magnetic moments of the i-th Cr atom in the upper layer and the j-th Cr atom in the lower layer, respectively. The nearest, second nearest and third nearest neighbors are represented by different colored lines in Fig. 4(c). Magnetic force theory is needed to analyze the magnetic interaction between layers to obtain the interaction parameters of magnetic atoms in the nearest neighbor.

Here, we obtain the exchange parameter J between different Cr atoms in the interlayer by OpenMX [29,30] soft-

ware. We take the AA-stacking as an example. In combination with Figs. 4(b) and 4(c), the interaction between the two Cr atoms in the upper and lower layers nearest to each other in the protocell is defined as J_1, and the second nearest is defined as J_2. Because of their different interaction properties, we divide the third nearest Cr atom into J_3 and J_3'. The lines of different colors in Fig. 4(c) correspond to the lines in Fig. 4(b). The minus and positive values represent AFM and FM interactions, respectively. We can see that the AFM interaction between layers is relatively weak when the lattice constant is 7 Å. However, with the increase of the lattice constant, only the J_3 rises slightly, and the other exchange parameters all decline, and J_1 drops particularly significantly. In the $\pi/3$-twisted bilayer CrI_3, the interlayer exchange interaction is in the range from -1.2 to 0.2 meV. Similarly, in the study on bilayer CrI_3,[31] the value range for the interlayer interaction is from -0.3 to 1.5 meV. They are close to the range from -1.5 to 0.5 meV in $CrI_3/CrSe_2$ of the present work. This result explains why the increase of lattice constant leads to the coupling transition of material.

In conclusion, we have investigated the interlayer interaction in the heterostructure composed of CrI_3 and $CrSe_2$ monolayers. Through DFT calculations, the effects of strain and in-plain interlayer shifts on stacking energy and exchange energy are explored. The results show that shifting along the $[1\bar{1}0]$ direction can lead to a transition from AFM coupling to FM coupling. On the other hand, shifting along the [100] direction does not result in FM coupling. Additionally, the magnetic interaction between layers is found to be very sensitive to in-plain strain. A small compressive strain causes all stacking structures to exhibit interlayer FM coupling. Our calculation results provide a theoretical reference for experimental studies of interlayer magnetic interactions in heterostructures, and our research shows that this $CrI_3/CrSe_2$ heterojunction has potential applications in nanodevices.

Acknowledgments. This work was supported by the National Natural Science Foundation of China (Grant Nos. 12074213, 11574108, 12104253, 12104034, 12022415, and 12374054), the Major Basic Program of Natural Science Foundation of Shandong Province (Grant No. ZR2021ZD01), and the Project of Introduction and Cultivation for Young Innovative Talents in Colleges and Universities of Shandong Province.

References

[1] Novoselov K S, Geim A K, Morozov S V, Jiang D, Zhang Y, Dubonos S V, Grigorieva I V, and Firsov A A 2004 *Science* **306** 666
[2] Huang B, Clark G, Navarro-Moratalla E, Klein D R, Cheng R, Seyler K L, Zhong D, Schmidgall E, McGuire M A, Cobden D H, Yao W, Xiao D, Jarillo-Herrero P, and Xu X 2017 *Nature* **546** 270
[3] Gong C, Li L, Li Z L, Ji H W, Stern A, Xia Y, Cao T, Bao W, Wang C Z, Wang Y, Qiu Z Q, Cava R J, Louie S G, Xia J, and Zhang X 2017 *Nature* **546** 265
[4] Li B, Wan Z, Wang C, Chen P, Huang B, Cheng X, Qian Q, Li J, Zhang Z, Sun G, Zhao B, Ma H, Wu R, Wei Z, Liu Y, Liao L, Ye Y, Huang Y, Xu X, Duan X, Ji W, and Duan X 2021 *Nat. Mater.* **20** 818
[5] Kim H H, Yang B W, Li S W *et al.* 2019 *Proc. Natl. Acad. Sci. USA* **116** 11131
[6] Jiang S, Shan J, and Mak K F 2018 *Nat. Mater.* **17** 406
[7] Huang B, Clark G, Klein D R, MacNeill D, Navarro-Moratalla E, Seyler K L, Wilson N, McGuire M A, Cobden D H, Xiao D, Yao W, Jarillo-Herrero P, and Xu X 2018 *Nat. Nanotechnol.* **13** 544
[8] Seyler K L, Zhong D, Klein D R *et al.* 2018 *Nat. Phys.* **14** 277
[9] Klein D R, MacNeill D, Lado J L *et al.* 2018 *Science* **360** 1218
[10] Kumar Gudelli V and Guo G Y 2019 *New J. Phys.* **21** 053012
[11] Sun Z, Yi Y, Song T, Clark G, Huang B, Shan Y, Wu S, Huang D, Gao C, Chen Z, McGuire M, Cao T, Xiao D, Liu W T, Yao W, Xu X, and Wu S 2019 *Nature* **572** 497
[12] Guo K, Deng B, Liu Z, Gao C, Shi Z, Bi L, Zhang L, Lu H, Zhou P, Zhang L, Cheng Y, and Peng B 2020 *Sci. China Mater.* **63** 413
[13] Sivadas N, Okamoto S, Xu X, Fennie C J, and Xiao D 2018 *Nano Lett.* **18** 7658
[14] Yu H, Zhao J, and Zheng F 2021 *Appl. Phys. Lett.* **119** 222403
[15] Wang Z, Gutiérrez-Lezama I, Ubrig N, Kroner M, Gibertini M, Taniguchi T, Watanabe K, Imamoğlu A, Giannini E, and Morpurgo A F 2018 *Nat. Commun.* **9** 2516
[16] Song T, Cai X, Tu M W Y, Zhang X, Huang B, Wilson N P, Seyler K L, Zhu L, Taniguchi T, Watanabe K, McGuire M A, Cobden D H, Xiao D, Yao W, and Xu X 2018 *Science* **360** 1214
[17] Yang W, Yang X, Li M, Hu L, and Zheng F 2024 *Appl. Phys. Lett.* **124** 021901
[18] Shang J, Tang X, Tan X, Du A, Liao T, Smith S C, Gu Y, Li C, and Kou L 2020 *ACS Appl. Nano Mater.* **3** 1282
[19] Hohenberg P and Kohn W 1964 *Phys. Rev.* **136** B864
[20] Kohn W and Sham L J 1965 *Phys. Rev.* **140** A1133
[21] Perdew J P, Burke K, and Ernzerhof M 1996 *Phys. Rev. Lett.* **77** 3865
[22] Hobbs D, Kresse G, and Hafner J 2000 *Phys. Rev. B* **62** 11556
[23] Blöchl P E 1994 *Phys. Rev. B* **50** 17953
[24] Anisimov V I, Zaanen J, and Andersen O K 1991 *Phys. Rev. B* **44** 943
[25] Grimme S, Antony J, Ehrlich S, and Krieg H 2010 *J. Chem. Phys.* **132** 154104
[26] Kresse G and Furthmüller J 1996 *Phys. Rev. B* **54** 11169
[27] Zhang Z, Ni X, Huang H, Hu L, and Liu F 2019 *Phys. Rev. B* **99** 115441
[28] Huang M, Rugheimer P, Lagally M G, and Liu F 2005 *Phys. Rev. B* **72** 085450
[29] Boker S, Neale M, Maes H, Wilde M, Spiegel M, Brick T, Spies J, Estabrook R, Kenny S, Bates T, Mehta P, and Fox J 2011 *Psychometrika* **76** 306
[30] Liechtenstein A I, Katsnelson M I, Antropov V P, and Gubanov V A 1987 *J. Magn. Magn. Mater.* **67** 65
[31] Jang S W, Jeong M Y, Yoon H, Ryee S, and Han M J 2019 *Phys. Rev. Mater.* **3** 031001